Pore-scale investigation of viscous coupling effects for two-phase flow in porous media

Huina Li, Chongxun Pan, and Cass T. Miller
Center for the Integrated Study of the Environment, Department of Environmental Sciences and Engineering, Box 7431, University of North Carolina, Chapel Hill, North Carolina 27566-7400, USA
(Received 28 January 2005; published 29 August 2005)

Recent studies have revealed that viscous coupling effects in immiscible two-phase flow, caused by momentum transfer between the two fluid phases, can be important in porous medium systems. In this work, we use a three-dimensional parallel processing version of a two-fluid-phase lattice Boltzmann (LB) model to investigate this phenomenon. A multiple-relaxation-time (MRT) approximation of the LB equations is used in the simulator, which leads to a viscosity-independent velocity field. We validate our model by verifying the velocity profile for two-phase flow through a channel with a square cross section. We then simulate co-current flow through a sphere-pack porous medium and obtain correlations of the relative permeabilities as a function of capillary number, wettability, and the fluid viscosities. The results are qualitatively consistent with experimental observations. In addition, we calculate the generalized permeability coefficients and show that the coupling coefficients are significant and the matrix is nonsymmetric. We also find a strong correlation between the relative permeability and interfacial area between fluids, indicating that both the common extension of Darcy's Law and the generalized formulation accounting for viscous coupling effects do not provide adequate insight into two-phase flow processes in porous media. This work lends additional support for the hypothesis that interfacial area is a key variable for multiphase flow in porous medium systems.

DOI: 10.1103/PhysRevE.72.026705 PACS number(s): 47.11.+j, 47.55.Mh, 47.15.Gf

I. INTRODUCTION

Simultaneous two-fluid-phase (hereinafter two-phase) flow in porous medium systems occurs routinely in nature and is of significant interest in many environmental and industrial processes, including enhanced oil recovery and remediation of hazardous waste sites by nonaqueous phase liquid (NAPL) spills. While the use of the conservation of the mass equation to represent the flow systems are fundamental, the closure relations employed to complement the balance are empirical. The conventional closure of the system relies upon the use of relative permeabilities of each of two fluids from an extension of Darcy's Law for single-phase flow, instead of a formal conservation of momentum. However, Darcy's Law is strictly valid only for creeping single-phase flow [1]. For two-fluid-phase systems, the conventional view implies that the flows of the two fluids are essentially uncoupled and that the pressure gradient and gravity are the only driving forces for each individual fluid. The existence of viscous coupling between the two immiscible fluids, due to the momentum stress being transferred across the fluid-fluid interfaces [2–4], makes the simple extension of Darcy's Law highly questionable. Another assumption of the conventional Darcy's Law under serious challenge is that the relative permeability is a function of the corresponding fluid saturation only. It has been posited that two-phase flow depends upon many flow parameters, such as fluid saturations, capillary number, wettability, and the viscosity ratio between the nonwetting and wetting phases. Viscous coupling of the fluids is affected by each of these factors [5–8].

The majority of theoretical approaches [9–17] intended to improve upon the traditional two-phase flow model have led to a similar generalized model for two-phase flow that accounts for interfacial viscous coupling effects. In the generalized model, the flow of each fluid phase is a linear function of gradients of both phases, indicating that in two-phase flow systems, fluid flow will depend not only on the corresponding pressure gradient and body forces for the fluid of concern, but also on the corresponding terms for the companion fluid. This model results in four generalized coefficients, which are commonly referred to as generalized relative permeability coefficients. While there have been various experimental studies showing that the coupling coefficients are important for a range of porous medium flow problems [5–7,18], measurement techniques of the generalized coefficients are highly distinctive and the validity and reliability of the obtained results are in many cases questionable [19,20]. In addition, the model has not succeeded in resolving the complexity of two-phase flow through porous media. The generalized flow theory fails on two counts. First, the theory is of the Onsager-type; however, the controversial issue regarding whether or not the two cross coefficients are equal has not been settled [2]. Second, the generalized relative permeability coefficients depend strongly on capillary number, equilibrium contact angle, and the fluid saturation history [5,20], which is also the case with the traditional two-phase flow model.

Recently, a consistent and systematic approach, referred to as the thermodynamically constrained averaging theory (TCAT) approach, has been proposed for modeling multiphase flow [21,22]. The approach is based upon a complete and rigorous set of conservation equations that are closed with a set of relations that account for the effects of interfaces formed at the junction of two phases, rather than ad hoc empirical relations [11]. One of the conclusions from this approach is that the interfacial area between phases is an important variable that must be incorporated into a complete two-phase flow model. While there have been active research efforts devoted to test this theory [23–30], the evolving theory still requires improved experimental and small-scale

computational approaches to determine the appropriate microscale processes and closure relations.

The overall goal of this work is to investigate quantitatively the viscous coupling phenomenon of two-phase flow in a porous medium from a microscopic pore-scale perspective, where detailed information, such as the pore morphology and topology, is available. The specific objectives of this work are to

(1) review the research conducted to date on viscous coupling effects for two-phase flow in porous medium systems from theoretical, experimental, and computational efforts;

(2) advance a multiple-relaxation time (MRT) LB model capable of simulating two-phase flow in three-dimensional porous medium systems;

(3) validate our model by simulating a simple case of two-phase flow in which a theoretical solution that explicitly accounts for the interfacial coupling is available;

(4) investigate the effect of capillary number, wettability, and viscosity ratio on the conventional relative permeabilities in co-current two-phase flow through a sphere-pack porous medium;

(5) develop and execute a strategy to calculate the coupling coefficients in the generalized model; and

(6) investigate the hypothesis advanced in the TCAT approach that interfacial area is a critical variable in multiphase porous medium systems.

II. BACKGROUND

A. Theoretical developments

The traditional model describing the flow of two immiscible fluid phases under steady-state conditions relies upon an extension of Darcy's Law, written as

$$\boldsymbol{v}_i = -\frac{\kappa\kappa_{r,i}}{\mu_i}(\boldsymbol{\nabla} p_i - \rho_i \boldsymbol{g}), \tag{1}$$

where $\boldsymbol{v}_{i(i=w,n)}$ is the Darcy velocity for the wetting phase and nonwetting phase, p_i is the fluid pressure, $\rho_i \boldsymbol{g}$ is the body force, μ_i is the dynamic viscosity of the fluid, κ is the intrinsic permeability determined by the pore structure of the porous medium alone, and $\kappa_{r,i}$ is the relative permeability that depends upon fluid saturations, or fraction of the pore space occupied by each fluid, and potentially other factors.

As viscous coupling effects have been increasingly recognized, several theoretical approaches have been adopted to describe viscously coupled multiphase flow in porous medium systems. Bachmat and Bear [9], de la Cruz and Spanos [10], Gray [11], Hassanizadeh and Gray [12–14], and Whitaker [17] applied a volume averaging method to Stokes equation to arrive at a modified theory that includes viscous coupling effects between two fluid phases. Kalaydjian [15,16], on the other hand, used the ideas of irreversible thermodynamics to develop analogous transport equations describing immiscible two-phase flow in isotropic media.

These different theoretical approaches produced a similar final formulation that we will refer to as the generalized two-phase flow model, which may be written as

$$\begin{bmatrix} \boldsymbol{v}_w \\ \boldsymbol{v}_n \end{bmatrix} = -\begin{bmatrix} \kappa\kappa_{r,ww}/\mu_w & \kappa\kappa_{r,wn}/\mu_n \\ \kappa\kappa_{r,nw}/\mu_w & \kappa\kappa_{r,nn}/\mu_n \end{bmatrix}\begin{bmatrix} (\boldsymbol{\nabla} p_w - \rho_w \boldsymbol{g}) \\ (\boldsymbol{\nabla} p_n - \rho_n \boldsymbol{g}) \end{bmatrix}. \tag{2}$$

The generalized relative permeability coefficients include two conventional coefficients, $\kappa_{r,nn}$ and $\kappa_{r,ww}$, and two off-diagonal coefficients, $\kappa_{r,nw}$ and $\kappa_{r,wn}$.

One view of Eq. (2) is that this expression is a macroscale application of Onsager's fundamental reciprocity relation [31,32], which is the basis of the thermodynamics of irreversible processes at the microscopic level. According to Onsager's theorem, the cross coefficients, $\kappa_{r,nw}$ and $\kappa_{r,wn}$ in this case, are symmetric given a linear relationship between the forces and fluxes for an irreversible process. However, there has been diversity in opinions regarding whether or not Onsager's reciprocity relations of irreversible thermodynamics for microscopic systems are applicable to macroscopic viscous coupling phenomena. Among those who argue in favor of the applicability of Onsager's theory to coupled flows in porous media are Gunstensen and Rothman [33], Kalaydjian [15,16], Rose [34,35], and Auriault and Lewandowska [36]. Opposing views, however, are to be found in Avraam and Payatakes [5–7], Bentsen [37], Bentsen and Manai [38], Dullien and Dong [18], Goode and Ramakrishnan [39], and Bentsen [3]. They argue that the nature of two-phase porous medium flow is not amenable to the Onsager-type relation, due to the fact that the coupling permeability coefficients are complex functions of the characteristics of the flow systems and are dependent on many nonlinear pore-scale flow processes.

Recently, the TCAT approach has been advanced as a rigorous basis for the development of models of flow and transport phenomena in porous medium systems [21,22], which is the evolution of formal constrained averaging theory work that has been ongoing for many years [11,12,40–44]. This approach starts from microscopic balance equations of mass, momentum, and energy for two fluid phases, a solid phase, and the interfaces between the phases. Averaging theorems and geometric constraints are used to simplify the entropy inequality and guide the development of closure relations needed to yield well-posed models. As a result of this work, the importance of fluid-fluid interfaces in multiphase systems has been distinguished and incorporated in model formulations. Interfacial areas are considered as additional averaged macroscale variables that represent additional information related to the microscopic state of the system, such as the evolution of the distribution of fluids in the pore space. The importance of taking interfacial areas into account, including the potential to remove hysteresis from capillary pressure-saturation closure relations, has been demonstrated by several studies [29,45,46]. However, interfacial areas are not explicitly a part of either the traditional multiphase flow model or the generalized flow model.

B. Experimental investigations

Standard methods for measuring conventional relative permeabilities rely upon steady-state, uniform flow and constant capillary pressure gradients for both phases without gravitational effects. However, these approaches are unable

TABLE I. Summary of the experimental investigations of viscous coupling effects.

Investigators	Dim.	Medium	Experimental method	$\max\left(\frac{\kappa_{r,nw}}{\kappa_{r,nn}}\right)$	$\frac{\kappa_{r,nw}}{\kappa_{r,wn}}=1$
Kalaydjian[a]	3	Capillary tube	Co-current steady-state	70%	Yes
Bestsen and Manai[b]	1	Sandpack	Co-current and counter-current steady-state	>15%	No
Liang and Lohrenz[c]	1	Sandpack	Combination of steady-state and unsteady-state	70%	Yes
Dullien and Dong[d]	1	Sandpack	Co-current steady-state	35%	No
Avraam and Payatakes[e]	2	Pore network	Co-current steady-state	120%	No

[a]Reference [16].
[b]Reference [84].
[c]Reference [50].
[d]Reference [18].
[e]References [5–7].

to discern the values of the diagonal coupling coefficients. Seeking a suitable method to measure all four relative permeabilities in the general model is difficult. Limited numbers of experimental studies have attempted to do so, and a summary of these studies is reported in Table I.

Generally, three types of experiments are conducted to measure the permeability coefficients: steady-state [5–7,16,18,19,38,47], unsteady-state (so-called immiscible displacement) [48,49], and a combination of steady-state and unsteady-state [50]. The immiscible displacement experiments are the least time-consuming, allowing values of relative permeability and capillary pressure to be determined dynamically. However, these approaches are subject to uncertainties and measurement errors, which are caused by varying capillary pressure gradients and saturation gradients.

Steady-state experiments, on the other hand, are more popular among experimental investigators because the fluid saturations, flow rates, and pressure gradients in the system can be directly measured, making them seem more reliable. Several experiments, such as those by Dullien and Dong [18] and Zarcone and Lenormand [51] on sand packs, were performed by applying external force to only one fluid, so that the first two coefficients were determined and then alternately the other two coefficients were determined. Another approach, in which co-current flow is first applied by adding equal external forces to both fluids and then counter-current flow by adding the opposite forces, were explored in, for example, Bentsen and Manai [38].

A more systematic and complete set of experimental work was pursued by Payatakes' group [5–7,52–54], who performed experiments on a two-dimensional glass pore network model on a square lattice. Fluids with constant flow rates were injected through the medium co-currently until steady-state conditions were achieved. By varying the ratio of flow rates and pairs of fluids, relative permeability coefficients as a function of capillary number, wettability, viscosity ratio, and ratio of injecting flow rates were investigated, and a strong correlation between the macroscopic permeabilities and the steady-state pore-scale flow mechanisms was reported based on the capillary number in the flow system.

As the importance of interfacial area has been increasingly recognized, experimental measurement techniques have been developed to measure such quantities [27,55,56]. However, due to the difficulty in determining the four relative permeability coefficients in the generalized model and measuring the interfacial area, to the best of our knowledge no experimental study has appeared that has investigated the relationship between viscous coupling in two-phase flow and interfacial area.

C. Computational simulations

Since experimental work that aims to explore all the related flow characteristics is difficult to perform, current experimental studies on viscous coupling effects are all limited to one- and two-dimensional systems. On the other hand, numerical simulations, having benefited from the dramatic evolution of computational capabilities and new algorithms, have significant promise for helping advance fundamental understanding of viscous coupling theory and for guiding the design and interpretation of experimental studies. However, compared to laboratory experimental approaches, investigative studies to investigate viscous coupling using numerical means are extremely limited. Conventional numerical investigations using, for example, finite-difference and finite-element methods are even more scarce [34,57] because of difficulties associated with pore-scale simulation of multiphase flow using such techniques.

Recently, the lattice Boltzmann (LB) method [58,59], a relatively new method derived from its precursor, the lattice-gas cellular automata method [60,61], has grown in popularity in the field of computational fluid dynamics, because it provides a means of simulating true flow mechanisms with a realistic pore geometry for multiphase flow. It also allows more versatility in the choice of parameters than can be had in experiments and provides detailed information about flow processes at the microscale. However, only a few published studies have investigated viscous coupling effects using

these methods. Olson and Rothman [62] attempted to estimate the coupling coefficient using a lattice-gas model in a digitized rock geometry obtained by x-ray microtomography [63]. Langaas and Papatzacos [64] simulated co-current and counter-current steady-state flows at different wettabilities, viscosity ratios, and driving forces using a Bhatnagar-Gross-Krook (BGK), single-relaxation-time lattice Boltzmann model for a two-dimensional, uniform pore space.

Gunstensen and Rothman [33] used a BGK color-gradient lattice Boltzmann model to simulate two-phase flow in a three-dimensional porous medium. They delineated regions of linearity and nonlinearity between Darcy velocities and and forcing as a function of fluid saturations, and they observed Onsager reciprocity in the linear region where a relatively high body force was applied. However, some significant issues still remain unresolved: (1) the applicability of Onsager theory in the nonlinear regime, which represents flow in the majority of hydrological applications; (2) the consideration of porous medium systems with more realistic pore structure than those considered to date; and (3) application of modern, high-resolution LB methods. The studies mentioned above, although limited in number, provide motivation for a more complete study.

Another important aspect of viscous coupling is to elucidate the role of interfacial effects, as several researchers have realized [5,6,33]. By applying the LB model at the microscopic pore scale, the interfacial area between fluid phases can be readily determined. A marching cubes algorithm has been used extensively as a tool to resolve graphical interfaces [65–67]. Recently, a modified marching cubes (MMC) algorithm has been successfully implemented and used to compute interfacial area using data sets obtained directly from LB simulations [68]. This approach provides a means to investigate the dependence of relative permeabilities on the interfacial area and to evaluate the validity of evolving theories.

III. LATTICE BOLTZMANN MODEL

A. LB-MRT model

The LB method involves solving the microscopic Boltzmann equation, which can be viewed as a discrete approximation of the incompressible Navier-Stokes equations based on kinetic theory [69]. In the LB method, fluid flow is represented by the distribution functions of fluid particles moving on a regular lattice. The so-called D3Q19 lattice was used in this work, where "D3" indicates three dimensions, and "Q19" indicates a 19-dimensional space with corresponding velocity vectors $\boldsymbol{e}_i$ $(i=0,1,\ldots,18)$.

The evolution of the fluid particle distributions is governed by the discrete Boltzmann equation [70]:

$$\boldsymbol{f}(\boldsymbol{x}+\boldsymbol{e},t+1)-\boldsymbol{f}(\boldsymbol{x},t)=\mathsf{S}[\boldsymbol{f}^{(\mathrm{eq})}(\boldsymbol{x},t)-\boldsymbol{f}(\boldsymbol{x},t)], \tag{3}$$

where the bold-face symbols denote Q-dimensional column vectors, e.g.,

$$\boldsymbol{f}(\boldsymbol{x},t)=[f_0(\boldsymbol{x},t),f_1(\boldsymbol{x},t),\ldots,f_{18}(\boldsymbol{x},t)]^T$$

is a vector of the distribution functions at lattice location $\boldsymbol{x}$ and time t. The left-hand side of Eq. (3) represents the advection term, denoting that the fluid particles $\boldsymbol{f}(\boldsymbol{x},t)$ simply propagate in space according to the velocity $\boldsymbol{e}$. The right-hand side of Eq. (3) represents the collision term, accomplished by a multiple-relaxation-time (MRT) approximation of the particle distribution functions towards their equilibria via a $Q\times Q$ full collision matrix S.

Equivalently, one can consider the collision process being carried out in moment space, instead of discrete velocity space. Given a set of discrete velocity vectors $\boldsymbol{e}$ and corresponding distribution functions $\boldsymbol{f}(\boldsymbol{x},t)$, a vector of moments $\boldsymbol{m}_i(i=0,1,\ldots,18)$ can be constructed by a projection of the distributions f through a linear transformation, i.e.,

$$\boldsymbol{m}=\mathsf{M}\boldsymbol{f};\quad \boldsymbol{f}=\mathsf{M}^{-1}\boldsymbol{m},$$

where M is an integer transformation tensor, constructed via the Gram-Schmidt orthogonalization procedure [70–72]. The moments are related to the conserved (hydrodynamic) and non-conserved (kinetic) physical properties, including the density, the momentum, the kinetic energy, the energy flux, and the viscous stress tensor. Hence, Eq. (3) can be written as

$$\boldsymbol{f}(\boldsymbol{x}+\boldsymbol{e},t+1)-\boldsymbol{f}(\boldsymbol{x},t)=\mathsf{M}^{-1}\hat{\mathsf{S}}[\boldsymbol{m}^{(\mathrm{eq})}(\boldsymbol{x},t)-\boldsymbol{m}(\boldsymbol{x},t)]. \tag{4}$$

The corresponding collision matrix $\hat{\mathsf{S}}=\mathsf{M}\cdot\mathsf{S}\cdot\mathsf{M}^{-1}$ in moment space is a diagonal matrix:

$$\hat{\mathsf{S}}=\mathrm{diag}(0,s_1,s_2,0,s_3,0,s_3,0,s_3,s_4,s_5,s_4,s_5,s_6,s_6,s_6,s_7,s_7,s_7), \tag{5}$$

where s_i are the collision (or relaxation) parameters, indicating that the collision process for each moment m_i is accomplished by a linear relaxation towards its equilibrium $m_i^{(\mathrm{eq})}$. The transformation tensor M and the functional forms of the equilibrium moments $\boldsymbol{m}^{(\mathrm{eq})}$ for the D3Q19 lattice are given in [70,71].

The values of the collision parameters s_i that correspond to the conserved moments are irrelevant because $m^{(\mathrm{eq})}(\boldsymbol{x},t)=m(\boldsymbol{x},t)$ for the conserved moments; here we set them to be zero. Also, some of the collision parameters are set to be identical values to preserve symmetry on the chosen lattice. The kinematic viscosity ν is then defined as

$$\nu=\frac{1}{3}\left(\frac{1}{s_4}-\frac{1}{2}\right)=\frac{1}{3}\left(\frac{1}{s_6}-\frac{1}{2}\right). \tag{6}$$

Note that the conventional BGK single-relaxation-time model is a special case of the generalized LB-MRT model, where the collision matrix is $\mathsf{S}=(1/\tau)\mathbf{I}$. Here $\tau=1/s_4$ is the single relaxation time and $\mathbf{I}$ is the identity matrix.

B. Two-phase LB model

A Shan-Chen multicomponent LB model [73] was used in this work. We provide a short description of the model below, and we refer readers to our previous work [74] for additional details. The evolution equation for fluid k (wetting or nonwetting fluid) is

$$\boldsymbol{f}_k(\boldsymbol{x}+\boldsymbol{e},t+1)-\boldsymbol{f}_k(\boldsymbol{x},t)=\mathsf{M}^{-1}\hat{\mathsf{S}}_k[\boldsymbol{m}_k^{(\mathrm{eq})}(\boldsymbol{x},t)-\boldsymbol{m}_k(\boldsymbol{x},t)]. \tag{7}$$

The macroscopic fluid density ρ_k, fluid velocity $\boldsymbol{v}_k$ and common velocity $\boldsymbol{v}$ are obtained by

$$\rho_k(\boldsymbol{x},t)=\sum_i f_{i,k}(\boldsymbol{x},t),$$

$$\boldsymbol{v}_k(\boldsymbol{x},t)=\sum_i f_{i,k}(\boldsymbol{x},t)\boldsymbol{e}_i/\rho_k(\boldsymbol{x},t),$$

$$v(\boldsymbol{x},t)=\sum_k(\rho_k\mathbf{v}_k s_{4,k})\Big/\sum_k(\rho_k s_{4,k}).$$

To simulate multiphase flow in porous media, long-range interactions of the form

$$\boldsymbol{F}_k=\boldsymbol{F}_{k,f\text{-}f}+\boldsymbol{F}_{k,f\text{-}s}+\rho_k\boldsymbol{g}_k \tag{8}$$

are included, where $\boldsymbol{F}_{k,f-f}$ is the fluid-fluid interaction force, $\boldsymbol{F}_{k,f\text{-}s}$ is the fluid-solid interaction force, and $\rho_k\boldsymbol{g}_k$ is the gravitational force for fluid k. Note that one can choose arbitrary values for the gravitational coefficient $\boldsymbol{g}_k$ to replace the desired fluid pressure gradient, which simplifies the handling of boundary conditions.

The change in momentum due to interaction forces $\boldsymbol{F}_k$ is included in the equilibrium function $\boldsymbol{m}_{i,k}^{(\mathrm{eq})}(\rho_k,\boldsymbol{v}_k^{\mathrm{eq}})$, where $\rho_k\boldsymbol{v}_k^{\mathrm{eq}}=\rho_k\boldsymbol{v}+\boldsymbol{F}_k/s_{4,k}$ [75]. In the model, nearest neighbor interactions are used to define the inter-particle forces. The fluid-fluid interaction force $\boldsymbol{F}_{k,f\text{-}f}$ on fluid k at site $\boldsymbol{x}$ is the sum of the forces between the fluid k particle at $\boldsymbol{x}$, and the fluid k' particles at neighboring sites $\boldsymbol{x}'$, given as

$$\boldsymbol{F}_{k,f\text{-}f}(\boldsymbol{x})=-\psi_k(\boldsymbol{x})\sum_{\boldsymbol{x}'}G(\boldsymbol{x},\boldsymbol{x}')\psi_{k'}(\boldsymbol{x}')(\boldsymbol{x}'-\boldsymbol{x}), \tag{9}$$

where $\psi_k(\rho_k)$ is a function of local density and for simplicity $\psi_k(\rho_k)=\rho_k$ is used in this study. In Eq. (9), G represents the strength of the interpartical force. By choosing G properly, fluids can separate so that immiscible multiphase flow behavior motivated by interfacial tension can be produced [76].

The interaction force $\boldsymbol{F}_{k,f\text{-}s}$ between the fluid k at site $\boldsymbol{x}$ and the solid at site $\boldsymbol{x}'$ is defined as

$$\boldsymbol{F}_{k,f\text{-}s}(\boldsymbol{x})=-\rho_k(\boldsymbol{x})\sum_{\boldsymbol{x}'}G_{ks}(\boldsymbol{x},\boldsymbol{x}')(\boldsymbol{x}'-\boldsymbol{x}). \tag{10}$$

Again, one can choose the sign and the magnitude of coefficient G_{ks} to distinguish the different wetting preferences of pure fluids. Detailed descriptions for choosing these coefficients for the fluid-fluid and fluid-solid interaction forces in the multiphase LB model were discussed in our previous work [74]. The overall fluid momentum is defined as [77]:

$$\rho\boldsymbol{u}=\sum_k\sum_i f_{i,k}\boldsymbol{e}_i+\frac{1}{2}\sum_k\boldsymbol{F}_k, \tag{11}$$

where $\boldsymbol{u}$ is the overall fluid velocity, and $\rho=\Sigma_k\rho_k$ is the total density of the fluids.

The LB method is a computationally intensive approach. As a result, an efficient parallel algorithm and implementation are critical for large-scale multiphase LB simulations. In this work, we adapted a LB implementation approach proposed by Pan *et al.* [78], which utilizes an orthogonal recursive bisection (ORB) decomposition that leads to excellent parallel efficiency by maintaining an efficient workload balance among subdomains.

IV. MODEL VALIDATION

A. Comparison between BGK and MRT model

In the LB method, no-slip velocity boundary conditions are usually approximated using the bounce-back scheme, which mimics the phenomenon that a particle reflects its momentum in some way when colliding with a solid surface. However, the actual position of a boundary is viscosity dependent when applying the BGK model [79,80]. While in the MRT model, the viscosity dependence can be eliminated by individually adjusting the collision parameters.

In order to illustrate the benefit of the MRT model over its BGK counterpart, we performed a test for single-phase flow through a homogeneous sphere-pack porous medium, labeled as GB1b. The porosity of the GB1b medium was 0.36 and the relative standard deviation of the spherical grain size was 10.1%; more properties of the GB1b medium were given in [74]. We used a subset of the entire GB1b sphere pack and discretized it using a $64\times64\times32$ lattice. A mirror image was created along the flow direction to enforce periodic boundary condition. The resulting medium contained about 150 spheres with 64^3 lattice nodes, corresponding to 13 lattice nodes per average sphere diameter. This discretization level was chosen based upon our previous investigations [74], which showed that for the same sphere-pack porous medium, the simulated relation curve between capillary-pressure and saturation in a NAPL-water flow system approaches convergence if the number of lattice nodes per average sphere diameter $\zeta\geqslant13.0$.

In the MRT model, s_4 and s_6 were determined based on Eq. (6), and following the analysis by Ginzburg and d'Humières [79], we used

$$s_1=s_2=s_5=s_4,\quad s_3=s_7=8(2-s_4)/(8-s_4) \tag{12}$$

in order to minimize the permeability dependence on viscosity. By applying a constant body force to the flow through the medium, we calculated the steady-state Darcy velocity and estimated the saturated permeability of the medium with respect to different fluid viscosities (i.e., $\tau=0.6,0.8,1.0,1.5$) using both the MRT and BGK models. As shown in Fig. 1, the simulated permeability obtained by the BGK model increases significantly with increasing viscosities, although refining the discretization to 128^3 mitigated the level of dependence. We observed that the permeabilities obtained by the MRT model remained essentially constant for both the 64^3 and 128^3 discretization levels when the viscosity changed by a factor of 10. Therefore, compared to BGK models, MRT models are more suitable for application to multiphase flow systems, where fluids of varying viscosities are present simultaneously, and where applying fine enough discretization of pore geometries to achieve the desired accuracy is often computationally impractical.

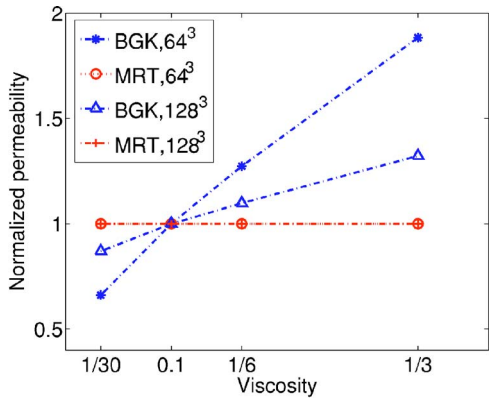

FIG. 1. (Color online) Comparison of the measured permeability of a sphere-pack porous medium as a function of fluid viscosities using BGK and MRT models. The permeability results are normalized with respect to the value at $\nu=0.1$.

B. Two-phase flow in a tube

We further validated the LB multiphase model by considering flows in a simple geometry for which a theoretical solution is available. Our simulation was performed in a three-dimensional tube with a square cross section, filled with a nonwetting phase (NWP) of viscosity ν_n and a wetting phase (WP) of viscosity ν_w, as shown in Fig. 2(a). The configuration of the interface between the NWP and WP depends upon the radius of interface R, which is defined by the pressure difference between the fluids.

Semianalytical approximations of the solution that account for the interfacial stress balance between the NWP and WP were given by Ehrlich [8], who exploited the solution to investigate viscous coupling effects on a bundle of capillary tubes. Axial velocities for the NWP and WP are represented in polar coordinates by the series

$$\boldsymbol{v}_n(r,\theta) = -\frac{\nabla p_n - \rho_n g_n}{\mu_n}\left(-\frac{r^2}{4} + a_0 + \sum_{j=1}^{\infty}[a_j r^{sj}\cos(sj\theta)]\right),$$

$$\boldsymbol{v}_w(r,\theta) = -\frac{\nabla p_w - \rho_w g_w}{\mu_w}\left(-\frac{r^2}{4} + b_0 + \sum_{j=1}^{\infty}[(b_j r^{sj} + c_j r^{-sj})\cos(sj\theta)]\right) \quad (13)$$

where $\boldsymbol{v}_{i,(i=n,w)}$ is the fluid velocity of the NWP/WP phases along the flow direction, μ_i is the dynamic viscosity, s is the number of the sides of the cross section in polygon tubes (which is 4 for square cross-sections), and a_j, b_j, and c_j are the undetermined parameters. The series in Eq. (13) have to be truncated to a finite number at $j=N$ so that a total number of $3N+2$ unknown parameters ($a_{j,j=0,N}$, $b_{j,j=0,N}$, and $c_{j,j=1,N}$) need to be determined. We truncated the series at $N=15$, which led to a sufficiently small convergence error, according to the results reported in Ehrlich [8]. Hence, we solved for 32 unknown a's, b's, and c's from 32 equations constructed by applying a zero velocity boundary condition at the tube wall, and continuity of velocity and a stress balance

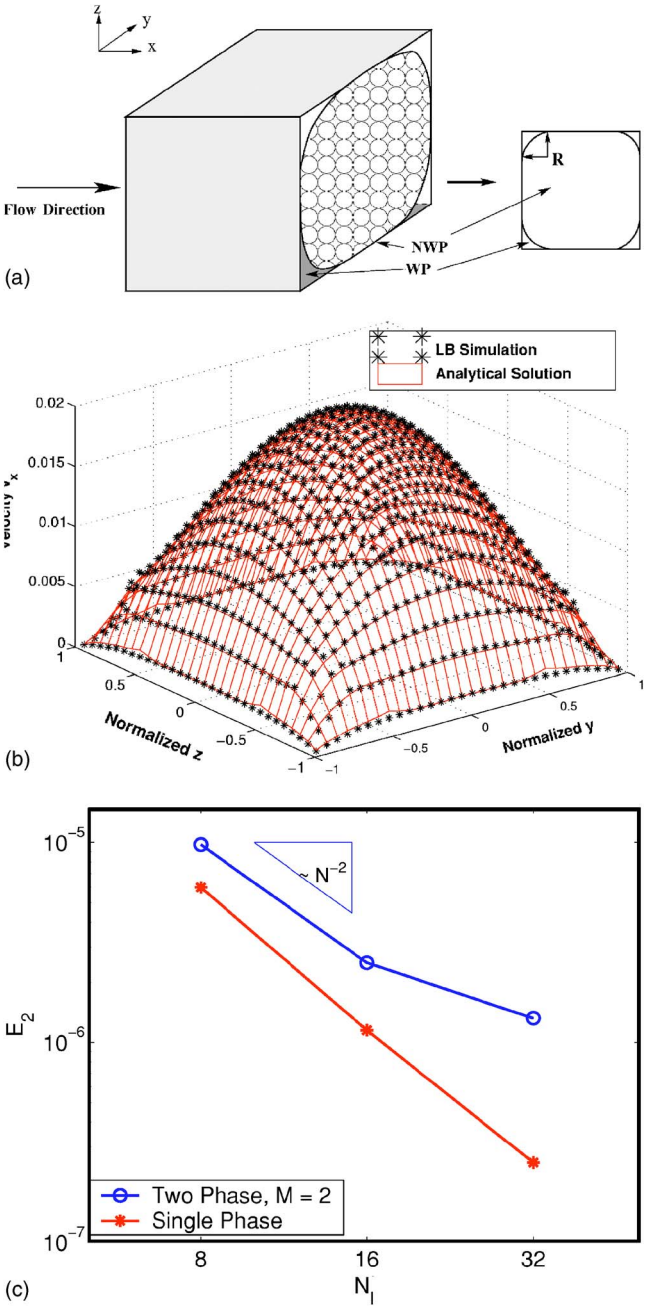

FIG. 2. (Color online) (a) Two-phase flow in a channel with square-shaped cross section; (b) Cross-sectional velocity profile for a phase viscosity ratio $M=2$ with 32^2 lattice nodes along the y-z plane; and (c) Error of the simulated velocity v_x profile with respect to the semianalytical solution versus lattice size N_l for single-phase flow and two-phase flow with a viscosity ratio $M=2$.

across the NWP-WP interface. We compared the velocity field obtained at $N=15$ with that obtained at $N=20$, and found that the L_2 norm of the difference between the two solutions was less than 6×10^{-8}, which confirmed the convergence of the velocity field.

In the LB simulation performed to compare to this analytical solution, the fluid-fluid interaction coefficient $G_{k'k}$ was set to 0.001, determined from a simple bubble test (see details in [74]) such that the desired phase separation was

produced. The fluid-solid interaction coefficients G_{ks} were set to zero because the interactions between both fluids and the wall were neglected in the analytical solution. Initially, both the NWP and WP were placed within the tube as shown in Fig. 2(a); the system was allowed to reach steady state after the body forces were imposed for both fluids. Periodic boundary conditions were applied in the x direction along the channel length, and steady state was considered to be achieved when the following criterion was satisfied:

$$\frac{\sqrt{\sum_{\boldsymbol{x}} [u_x(\boldsymbol{x},t) - u_x(\boldsymbol{x},t-50)]^2}}{\sqrt{\sum_{\boldsymbol{x}} u_x(\boldsymbol{x})^2}} < 10^{-5}, \tag{14}$$

where u_x is the overall fluid velocity [defined in Eq. (11)] along the flow direction x.

Figure 2(b) plots the steady-state profile of v_x in the middle plane of the channel with a radius of interface $R=10$, body forces $g_n=g_w=10^{-4}$, and a viscosity ratio $M=\nu_n/\nu_w=2$. A good agreement between the LB simulation and the analytical solution is illustrated in Fig. 2(b) using 32^2 lattice nodes in the y-z cross section. To further evaluate the difference between the numerical LB solution and the semianalytical solution, we calculated the L_2 norm error of velocity field, defined as

$$E_2 = \sqrt{\frac{\sum_{\boldsymbol{x}} [v_x(\boldsymbol{x}) - v_x^*(\boldsymbol{x})]^2}{N_l^3}}, \tag{15}$$

where v_x^* is the Ehrlich's semianalytical solution defined in Eq. (13), and N_l^2 is the number of lattice nodes in the y-z cross section. We observed a second-order rate of convergence for single-phase flow, whereas for coupled two-phase flow at $M=2$, we obtained an order of convergence of 1.4, which we calculated using linear regression to fit E_2 with respect to N_l in log space. The lower order of convergence for the coupled two-phase flow case was expected because of the interfacial effect caused by the steep gradient in density across the fluid-fluid interface [81,82]. We have observed similar rates of convergence for two-phase flow in a tube with M up to 5.

V. TWO-PHASE FLOW SIMULATIONS IN POROUS MEDIA

A. Setup of the numerical system

We used the identical porous medium and discretization approach detailed in Sec. IV A. To determine if our simulations were adequately resolved, we made spot checks by comparing the simulated relative permeabilities with 64^3 lattice nodes to a finer discretization with 96^3 lattice nodes and found that at the same saturation level the variation of the relative permeabilities between the two discretization levels for both fluid phases in the conventional model was within 5% in all cases.

We first determined the saturated permeability κ of the medium, which was calculated from a steady-state Darcy's velocity after applying a constant body force for one phase and setting the density of the other fluid equal to zero at all locations. It is important to note that the MRT model yields more accurate predictions of both saturated and relative permeabilities than the standard BGK model, which inherently has a relaxation-time dependent location of the no-slip boundary and thus leads to a viscosity dependent permeability.

Simulation of immiscible two-fluid-phase flow was performed as follows:

(a) Initially, both a NWP and WP of equivalent density were uniformly-distributed throughout the medium such that the desired WP saturation (denoted as S_w) was obtained;

(b) The medium was bounded by walls along the y and z directions and a periodic boundary condition was applied along the x direction;

(c) Co-current flow was simulated by adding body forces, as defined in Eq. (8), for both fluids along the flow direction. The reasons for using body forces instead of imposing a pressure gradient as a driving force are that: (1) using body forces can avoid capillary pressure gradients and thus saturation gradients along the flow direction; and (2) body forces are convenient to implement, since periodic boundary conditions can then be applied along the flow direction; and

(d) The fluid-fluid interaction coefficient G and fluid-solid coefficients G_{ks} were chosen such that the fluids with an assigned viscosity ratio were separated and the desired wettabilities were achieved [74]. For example, in a neutrally water-wet (NWW) system, the WP-solid and NWP-solid interaction coefficients were set to be -0.01 and 0.01, corresponding to a contact angle of approximately 65°, while in the strongly water-wet (SWW) system, those coefficients were set to be -0.02 and 0.02, corresponding to a contact angle of approximately 25°.

The conventional permeabilities for the NWP and WP were calculated following the extension of Darcy's law defined in Eq. (1). In order to calculate the four generalized permeability coefficients, one set of steady-state data is insufficient. Therefore, a second set of steady-state simulations was performed by perturbing the body force of the NWP by 20% of that used in the first set, while keeping the same body force for the WP. These conditions were important to provide similar flow conditions, yet sufficiently different conditions to allow determination of the four generalized permeability coefficients with sufficient accuracy.

In the following section, we first investigate the effects of capillary number, wettability, and viscosity ratio on the conventional permeabilities of fluids. We also calculate the generalized coefficients and investigate whether the generalized coefficient matrix is symmetric or nonsymmetric. Lastly, we investigate the correlation of the relative permeabilities as a function of the interfacial area.

B. Results and discussion

1. Effect of capillary number

We first show the dependence of the relative permeability on capillary number Ca, which describes the ratio of viscous forces to capillary forces:

$$\mathrm{Ca} = v_w \mu_w / \gamma. \tag{16}$$

The nondimensional interfacial tension γ can be obtained using Laplace's Law by means of a bubble simulation [74]. Figure 3 compares a series of snapshots of the NWP motion under two capillary numbers 5×10^{-4} [Figs. 3(a)–3(d)] and 5×10^{-5} [Figs. 3(e)–3(h)]. The corresponding Reynolds numbers of the WP

$$\mathrm{Re}=\rho_w v_w D/\mu_w \tag{17}$$

were 0.17 and 0.017, respectively, indicating a Darcy flow regime. In Eq. (17), D is the average diameter of solid grain in the medium.

For both cases, the driving force for the NWP was kept constant while the force for the WP in Figs. 3(a)–3(d) was one order of magnitude larger than that in Figs. 3(e)–3(h). The saturation of the NWP for both cases was 6%, which allowed us to track dynamically the movement of individual NWP regions. As illustrated in Fig. 3, the NWP was in the form of disconnected ganglia and trapped in big pores due to the resistance of capillary forces. At higher Ca, we observed the motion of disconnected NWP regions that had overcome the capillary resistance to movement. For example, the movement of a NWP region initially in the upper left of Fig. 3(a) was observed. However, this motion was undetectable in case of a lower Ca [see Figs. 3(e)–3(h)], although in both cases the driving body forces applied to the NWP were the same.

Strictly speaking, this is not a conventional steady-state scenario, although the macroscopic saturation and flow rates of both phases remain constant. The dynamic equilibrium of a moving disconnected NWP phase in "steady state" was first observed by Avraam *et al.* [52]. It is obvious that there is an interfacial momentum transfer from the WP, engulfing the disconnected NWP, to the NWP, which results in the mobilization of the disconnected NWP at higher Ca.

The influence of Ca on the conventional relative permeabilities is shown in Fig. 4, in which two levels of Ca's (Ca$=10^{-4}$ and Ca$=10^{-5}$) were compared in a neutrally wet porous medium. The body forces of the WP and NWP were kept equal ($g_n=g_w$) and were adjusted according to the WP velocity in order to achieve the desired Ca. This is similar to the way that the experiment by Avraam and Payatakes [7] was performed in glass pore networks. We found that both the NWP and WP permeability coefficients were increasing functions of Ca for the fluid system. This trend was also observed by Avraam and Payatakes [7] experimentally and by Langaas and Papatzacos [64] numerically.

In order to further investigate the effect of capillary number, we performed simulations at $S_w=0.5$ with different level of forcing and hence different Ca. Figure 5 shows that when Ca is 10^{-4} or smaller, the flow rate and the driving force exhibit highly nonlinear relations for both phases; while when Ca approaches 10^{-3}, the relative permeabilities are almost constant, indicating linear flows at high levels of forcing. This finding agrees with [33], despite differences between the porous media investigated and the LB simulators used. We note natural hydrologic two-phase flow systems are almost universally in the nonlinear regime because typically Ca$\ll10^{-4}$.

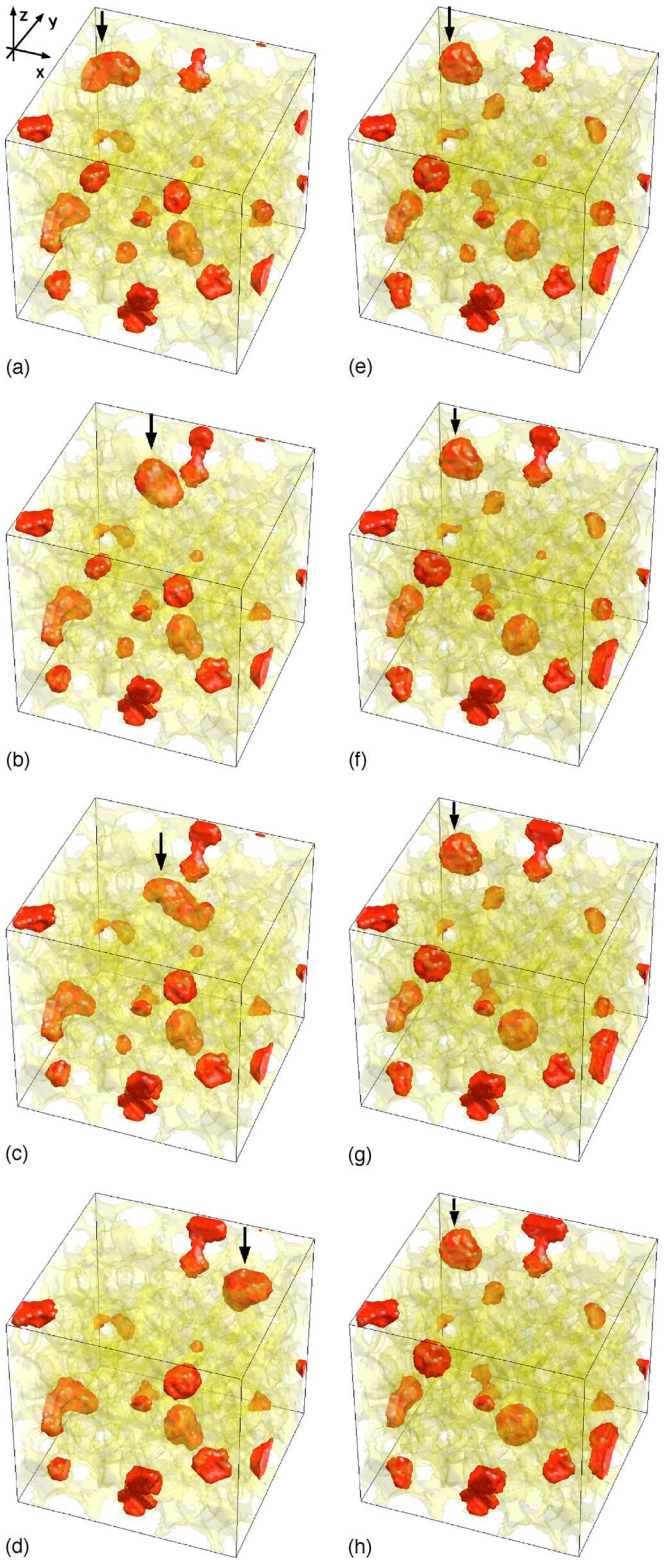

FIG. 3. (Color online) Snapshots of the nonwetting phase distribution under a higher capillary number [Ca$=5\times10^{-4}$, (a)–(d)] and a lower capillary number [Ca$=5\times10^{-5}$, (e)–(h)]. The NWP region indicated by the arrow in (a) moves through the porous medium driven by momentum transfered from the WP at higher Ca, while it is unable to move at lower Ca.

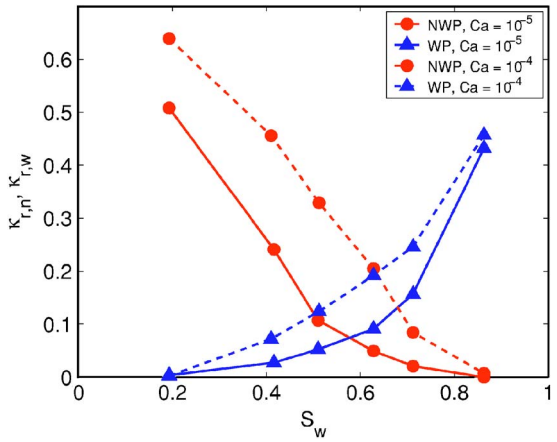

FIG. 4. (Color online) Relative permeability vs WP saturation S_w for co-current two-phase flow with different Ca in a neutrally wet medium at $M=1$.

2. Effect of wettability

Next, we studied the dependence of the relative permeability on wettability. Steady-state NWP distributions are illustrated in Fig. 6 for cases of neutrally water wet (NWW) and strongly water wet (SWW) media. For the case of a SWW medium, the NWP displaces the WP in the largest pores. Thus for the same saturation conditions, the NWP correspondingly occupies a set of larger pores on average for the SWW medium compared to the NWW medium. As a corollary to this observation, the NWP has a larger specific interfacial area with the solid phase, hence greater resistance to flow, in the NWW case than in the SWW case, which is consistent with previous observations [18]. On the other hand, the NWP becomes more disconnected in the SWW medium, as shown in Fig. 6. The former mechanism appears to be dominant because the total effect of these factors leads to a higher apparent NWP relative permeability in the SWW system than in the NWW system, as shown in Fig. 7. In particular, a substantially higher NWP relative permeability was observed in the SWW system than in NWW system at high NWP saturations, where the resistance effect of the

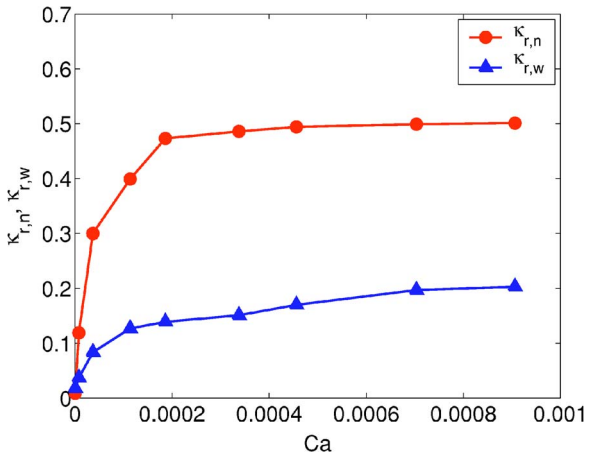

FIG. 5. (Color online) Relative permeabilities as a function of Ca for co-current, two-phase flow with $M=1$ and $S_w=0.5$.

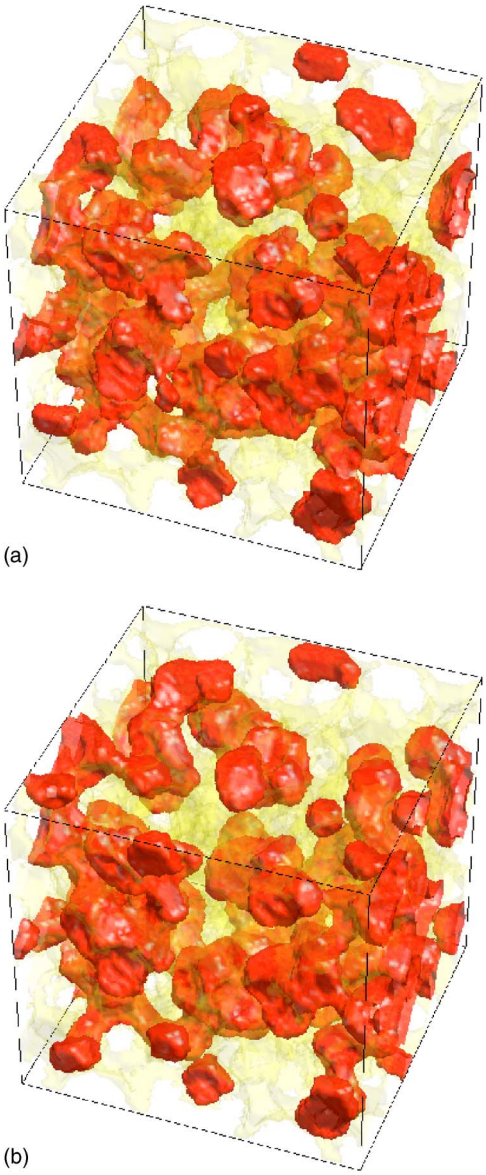

FIG. 6. (Color online) Steady-state distributions of the NWP (a) a neutrally wet medium; and (b) a strongly water-wet medium. Wetting-phase saturation $S_w=0.509$ in (a) and 0.508 in (b). Dark gray (red online) regions represent the nonwetting fluid, and light gray (yellow online) regions represent the solid phase. For clarity of illustration the wetting fluid is not shown.

solid phase boundary to the movement of NWP clearly outweighs the connectivity effect of the NWP in a SWW medium. This was also observed in experimental work reported in Dullien [83] for dolomite media and Avraam and Payatakes [6] for glass pore networks.

On the other hand, in a SWW system, due to the fact that NWP tends to occupy larger pores, the average size of pore space occupied by the WP is smaller for the SWW system compared to the NWW systems at a given saturation level. This would suggest that the WP relative permeability for a SWW system would be lower than the WP relative permeability in a corresponding NWW system. However, the WP is more connected in SWW media than in corresponding NWW media. Based upon our observations, the net effect of these

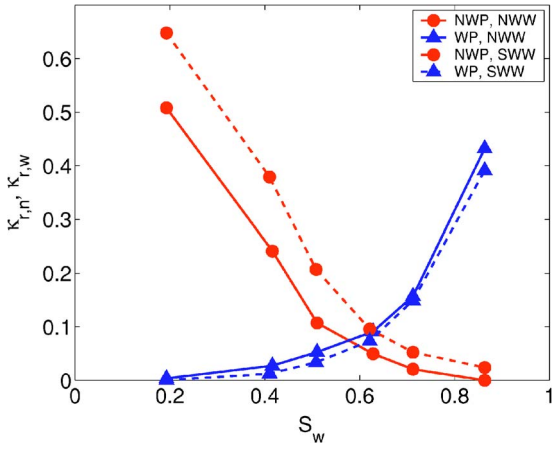

FIG. 7. (Color online) Relative permeability vs WP saturation S_w for co-current two-phase flow with different wettability with $M=1$ and $\mathrm{Ca}=10^{-5}$.

two off-setting mechanisms is a relatively small difference in the relative permeability of WP as a function of changes in wettability for the two conditions that we analyzed. This finding is in agreement with the experimental results reported in Avraam and Payatakes [7].

3. Effect of viscosity ratio

We further studied the dependence of the conventional relative permeabilities on the viscosity ratio between fluid phases. As experimental measurements of relative permeability data on three-dimensional porous medium systems are unavailable, we compared our simulations with Avraam and Payatakes's work [6], which was performed in a two-dimensional glass pore network. Figures 8 and 9 show these experimental data along with results of three-dimensional LB simulations used to measure conventional relative permeabilities as a function of WP saturation for two viscosity ratios, $M=1.45$ and $M=3.35$. From Fig. 8, we observe that

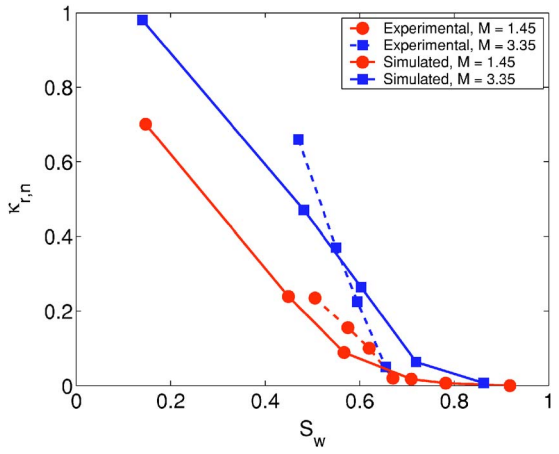

FIG. 8. (Color online) NWP relative permeability measured by [6] in a glass pore network with a contact angle of 40° and our simulated results for a NWW system as a function of WP saturation S_w for co-current, two-phase flow with different viscosity ratios at $\mathrm{Ca}=10^{-5}$.

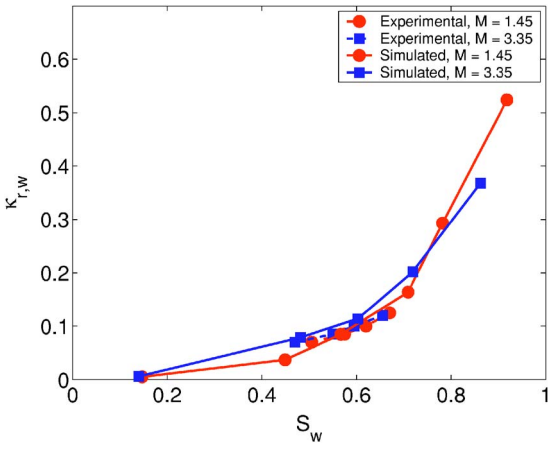

FIG. 9. (Color online) WP relative permeability measured by [6] in a glass pore networks with a contact angle of 40° and our simulated results in a NWW system as a function of WP saturation S_w for co-current, two-phase flow with different viscosity ratios at $\mathrm{Ca}=10^{-5}$.

an increased viscosity ratio M leads to a significantly increased NWP apparent relative permeability, especially when the saturation is in the intermediate range. This is because the WP, which is flowing in relatively small pore size connected paths and edges of the pore space, is strongly coupled to the NWP, which is flowing in the larger regions of the pore structure. As a result, the NWP experiences an apparent hydraulic slip, a so-called "lubricating" effect on the flow of the NWP due to the WP film [83]. The greater the viscosity of the NWP, or the ratio M, the greater the hydraulic slip becomes.

This macroscopic trend in relative permeability can also be due to changes in the NWP distribution as a function of M, as observed experimentally by [6] in their two-dimensional glass network, in which they found that a higher viscosity ratio favors a more connected NWP pathway and hence greater NWP permeability. It is also consistent with the numerical study done by Langaas and Papatzacos [64]. The different permeability values among investigators are due to differences in capillary numbers among the systems, medium morphology, fluid properties, or dimensionality effects.

On the other hand, the flow of a less viscous WP is effected less by the viscosity of the NWP, therefore the WP relative permeability is relatively insensitive to changes in M. This trend was clearly confirmed by our simulations and the experimental work of Avraam and Payatakes [6], as shown in Fig. 9.

4. Generalized permeability coefficients

The generalized permeability coefficients for the NWP and WP were calculated and are shown in Fig. 10. The magnitude of the $\kappa_{r,nw}$ coupling coefficient is comparable to the diagonal coefficient at intermediate saturations, which indicates that the interfacial viscous coupling in two-phase flow is an important phenomenon. Interestingly, $\kappa_{r,nw} > \kappa_{r,nn}$ for $S_w \geqslant 0.5$, which we attribute to the disconnected nature of the NWP in this region. This indicates that in such an instance

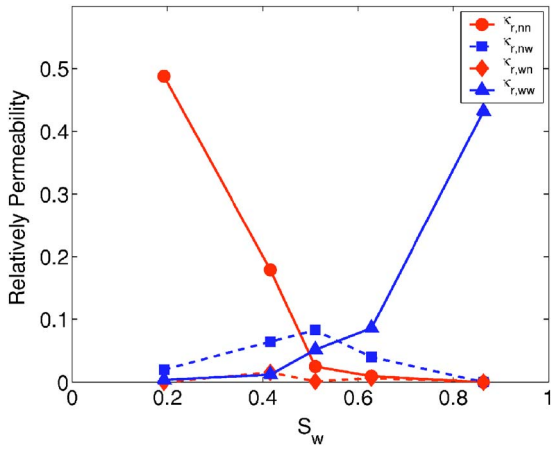

FIG. 10. (Color online) Generalized relative permeabilities as a function of WP saturation S_w for co-current two-phase flow with $M=1$ and $\mathrm{Ca}=10^{-5}$.

the movement of the NWP phase is assisted by the WP. Since $\kappa_{r,wn}>0$, this coupling also assists the flow of the WP, but to a significantly lesser extent. We hypothesize that these results are influenced by the distribution of interfacial areas for each of the fluid phases.

We found that the cross coefficients are nonequal and $\kappa_{r,nw}$ is generally greater than $\kappa_{r,wn}$. This provides evidence against the applicability of the Onsager's theory in two-phase porous medium flow at macroscale. This observation is consistent with the majority of the findings from recent investigations of viscous coupling effects [6,7,18]. The nonsymmetric cross coefficients are essentially caused by the difference in microscopic morphology and topology of the two fluids. In a SWW system with intermediate saturation, WP predominantly fills the thin channels and small pores that the NWP is not able to enter, while the rest of WP coexists with NWP in wider channels and larger pore spaces. Since the coupling effects only occur at the interfaces between the fluids, the influence of coupling on WP is smaller than that on NWP.

Our results, however, seemingly disagree with the computational study by Gunstensen and Rothman [33], who found that the Onsager reciprocity holds. However, Gunstensen's numerical experiments were conducted in the linear flow regime (i.e., where $\boldsymbol{v}_{w/n}$ is a linear function of the forcing) by enforcing high body forces, while our study was performed at $\mathrm{Ca}=10^{-5}$. For this Ca the flow rate and the driving force exhibit nonlinear relations for both phases, as discussed earlier in Sec. V B 1. We verified this by spot-checking the four generalized permeability coefficients at $S_w=0.5$ with $\mathrm{Ca}=10^{-3}$ using the same approach outlined in Sec. V A. We found that the coupling coefficients $\kappa_{r,nw}$ and $\kappa_{r,wn}$ differed by only 10% and they were both significant compared to the diagonal coefficients. This suggests that when capillary number is large, the generalized model is a reasonable model and is superior to the conventional Darcy's Law.

The identification of the linear and nonlinear regimes and the dependence of Onsager's reciprocity on these regimes also indicates that there might be different flow mechanisms dominating the flow phenomena when fluid velocities change significantly. While some studies have attempted to explain these flow mechanisms based on experimental [6,7] or computational [33] observations, distinction of these mechanisms was based on many flow parameters in the specific media used in these studies and no unified indicator or potential variable has been suggested. We believe further study along this line is important to fully understand the complicated flow phenomena in multiphase porous medium systems.

5. Effect of fluid-fluid interfacial area

We explored the effect of fluid-fluid interfacial area on relative permeabilities. Unlike previous simulations, we removed the solid walls that bound the medium along the y and z directions in order to eliminate the influence of the additional solid-fluid interfaces. Thus, periodic boundary conditions were used in all three directions, although the body force acted only in the x direction. Different spatial distributions of both fluids at a fixed saturation were achieved by initially distributing the fluids in different portions of the medium.

The resulting steady-state distributions of NWP are illustrated in Fig. (11). In Case 1 [Fig. 11(a)], the WP occupied primarily the top half of the medium and the NWP occupied primarily the bottom half; in Case 2 [Fig. 11(b)], the NWP was placed in the middle of the medium; while in Case 3 [Fig. 11(c)], the NWP was distributed uniformly throughout the medium. At steady state in each configuration, the interfacial area for each configuration was calculated using an MMC algorithm implemented by McClure *et al.* [68].

As a first attempt to investigate the effects of interfacial area, we evaluated the relation between the conventional relative permeability and interfacial area, holding fluid saturations essentially constant. Figure 12 indicates strong correlations between the relative permeabilities for NWP and WP and the fluid-fluid interfacial areas under the same saturation level. In Case 1, WP occupied the top half of the medium and NWP occupied the bottom half; thus generally, each phase flowed as a continuous phase and the interfacial area between the phases was smaller than that in other cases. Therefore, the relative permeability for each phase was higher in Case 1 than that in other cases. In Case 2, NWP still flowed as a continuous but slightly more scattered phase, while WP was divided into top and bottom parts, which led to a larger interfacial area between fluids and hence slightly decreased NWP and significantly decreased WP permeabilities. In Case 3, both the NWP and WP were the most disconnected. This was reflected by an increase in the interfacial area. As a result, the NWP and WP relative permeabilities decreased by 50% and 40% compared to Case (b), respectively. The sensitivity of the WP relative permeability with respect to changes in interfacial areas is especially striking. Based on the above results, we believe that interfacial area is an important measure of the morphology and topology of fluid distributions in macroscale porous medium systems, which is not accounted for in either the conventional or generalized relative permeability models. This provides additional evidence for the evolving TCAT approaches, which include interfacial areas as natural quantities in macroscale models [21,22].

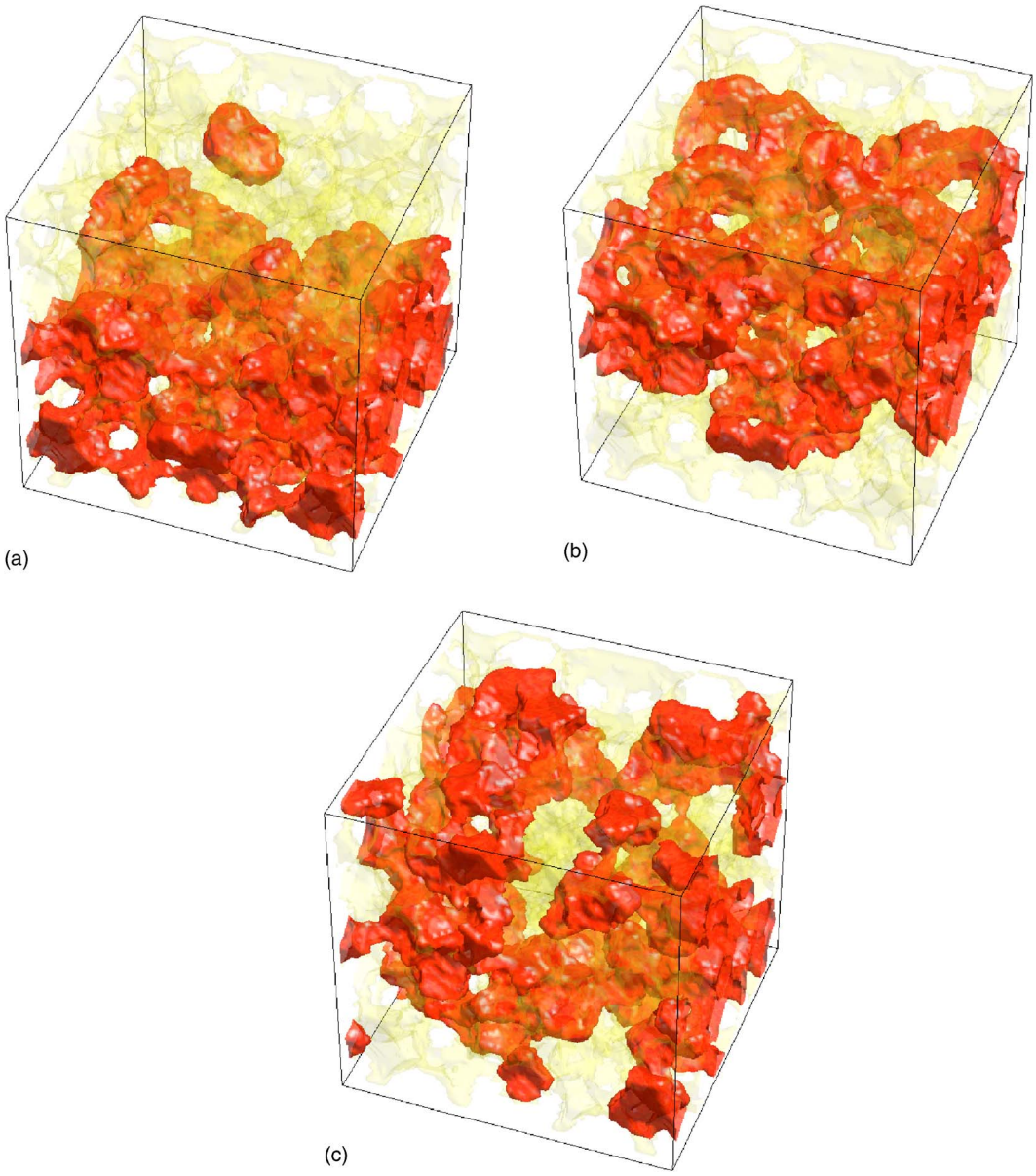

FIG. 11. (Color online) Steady-state distributions of NWP with different initial phase configurations: (a) Case 1, (b) Case 2, and (c) Case 3. For all cases, the WP saturation is 0.45–0.46.

VI. CONCLUSIONS

The LB method is a useful approach for studying the complex behavior of two-fluid-phase flow in porous media. Particularly, the ease of obtaining the local parameters, such as permeability, saturation, and flux, makes it suitable for use in exploring pore-scale physics within porous medium systems. In addition, we believe that the multiple-relaxation-time (MRT) LB models are superior to the BGK models for multiphase flow simulations, due to the fact that the MRT models improve the numerical stability and yield a viscosity-independent velocity field, which is impossible to achieve using the standard BGK models. The investigations of two-phase flow in a channel with a square-shaped cross section show good agreement with the analytical solution of axial fluid velocities using the LB-MRT model.

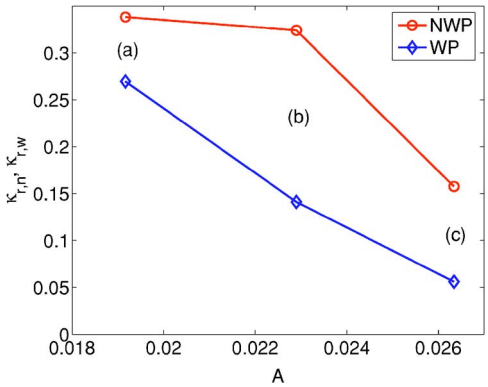

FIG. 12. (Color online) Conventional relative permeabilities of NWP and WP vs fluid-fluid interfacial area per unit volume at constant fluid saturations for (a) Case 1, (b) Case 2, and (c) Case 3.

Three-dimensional investigations of viscous coupling effects were carried out for two-fluid-phase flow through a sphere-pack porous medium. Viscous coupling effects were found to be important over a broad range of conditions, including capillary number, wettability, and viscosity ratio. Qualitative trends in the change of conventional permeability with the above parameters compare favorably with the experimental results obtained by Avraam and Payatakes [6,7]. The motion of disconnected NWP regions under higher Ca was captured, which indicates that the prevailing assumption that disconnected parts of a nonwetting fluid phase remain static is invalid under certain conditions.

The dependence of the permeability-saturation curve on the capillary number, wettability, and viscosity ratio provides evidence against the sole dependence of permeability on the corresponding fluid saturation posed in the conventional extended form of Darcy's Law. An attempt to calculate the coupling coefficients in the generalized formulation showed that viscous coupling effects contribute significantly to fluid flow. In addition, those coupling coefficients were found to be unequal, which implies that the Onsager's reciprocity relation is not applicable for describing multiphase flow in macroscale porous medium systems. We also note that most of our studies were performed for $\mathrm{Ca} < 10^{-4}$, as Ca at this range is of practical concern in subsurface systems. Other work found that Onsager theory was valid at higher Ca (still sufficiently low to fall into Darcy flow regime), which was confirmed by our study as well.

The evolving TCAT approach motivated us to further investigate the role of interfacial area for two-phase flow in porous media. A strong dependence of relative permeabilities on fluid-fluid interfacial area was found. For a fixed saturation level, different flow topologies resulted in significantly different relative permeabilities. This suggests that the distinguishing feature of multiphase flow systems—the existence of fluid-fluid interfaces, should be accounted for explicitly in a more complete model formulation. New models that overcome the deficiencies of the conventional and generalized theories deserve further study.

ACKNOWLEDGMENTS

The authors express their appreciation to William Gray for his inspiring suggestions and to James McClure and David Adalsteinsson for help with interfacial area calculations. This work was supported by National Science Foundation (NSF) Grant No. DMS-0327896 and Grant No. P42 ES05948 from the National Institute of Environmental Health Sciences.

[1] W. Rose, J. Petrol. **26**, 187 (2000).
[2] M. Ayub and R. G. Bentsen, J. Petrol. **23**, 13 (1999).
[3] R. G. Bentsen, J. Petrol. **21**, 27 (1998).
[4] R. G. Bentsen, J. Petrol. **19**, 177 (1998).
[5] D. G. Avraam and A. C. Payatakes, J. Fluid Mech. **293**, 207 (1995).
[6] D. G. Avraam and A. C. Payatakes, Transp. Porous Media **20**, 135 (1995).
[7] D. G. Avraam and A. C. Payatakes. Ind. Eng. Chem. Res. **38**, 778 (1999).
[8] R. Ehrlich, Transp. Porous Media **11**(3), 201 (1993).
[9] Y. Bachmat and J. Bear, Transp. Porous Media **1**(3), 213 (1986).
[10] V. de la Cruz and T. J. T. Spanos, Am. Inst. Chem. Eng. Symp. Ser. **29**, 854 (1983).
[11] W. G. Gray, Adv. Water Resour. **22**(5), 521 (1999).
[12] S. M. Hassanizadeh and W. G. Gray, Adv. Water Resour. **2**(3), 131 (1979).
[13] S. M. Hassanizadeh and W. G. Gray, Adv. Water Resour. **2**(4), 191 (1979).
[14] S. M. Hassanizadeh and W. G. Gray, Adv. Water Resour. **3**(1), 25 (1980).
[15] F. Kalaydjian, Transp. Porous Media **2**, 537 (1987).
[16] F. Kalaydjian, Transp. Porous Media **5**(3), 215 (1990).
[17] S. Whitaker, Transp. Porous Media **1**, 3 (1986).
[18] F. A. L. Dullien and M. Dong, Transp. Porous Media **25**(1), 97 (1996).
[19] E. Dana and F. Skoczylas, Int. J. Multiphase Flow **28**, 1719 (2002).
[20] W. Rose, Transp. Porous Media **3**(2), 163 (1988).
[21] W. G. Gray and C. T. Miller, Adv. Water Resour. **28**, 161 (2005).
[22] C. T. Miller and W. G. Gray, Adv. Water Resour. **28**, 181 (2005).
[23] M. E. Coles, R. D. Hazlett, E. L. Muegge, K. W. Jones, B. Andrews, B. Dowd, P. Siddons, A. Peskin, P. Spanne, and W. Soll, SPE Reservoir Eval. Eng. **1**(4), 288 (1998).
[24] D. W. Grunau, W. T. Lookman, S. Y. Chen, and A. S. Lapedes, Phys. Rev. Lett. **71**(25), 4198 (1993).
[25] R. D. Hazlett, Transp. Porous Media **20**(1–2), 21 (1995).
[26] R. D. Hazlett, S. Y. Chen, and W. E. Soll, J. Petrol. **20**(3–4), 167 (1998).
[27] C. D. Montemagno and W. G. Gray, Geophys. Res. Lett. **22**(4), 425 (1995).
[28] M. Rashidi, L. Peurrung, A. F. B. Tompson, and T. J. Kulp, Adv. Water Resour. **19**(3), 163 (1996).
[29] P. C. Reeves, and M. A. Celia, Water Resour. Res. **32**(8), 2345 (1996).
[30] D. Zhang, R. Zhang, S. Chen, and W. E. Soll, Geophys. Res. Lett. **27**(8), 1195 (2000).
[31] L. Onsager, Phys. Rev. **37**, 405 (1931).
[32] L. Onsager, Phys. Rev. **38**, 2265 (1931).
[33] A. K. Gunstensen and D. H. Rothman, J. Geophys. Res. & Solid Earth **98** (B4), 6431 (1993).
[34] W. Rose, Transp. Porous Media **5**(1), 97 (1990).
[35] W. Rose, Transp. Porous Media **18**(1), 87 (1995).
[36] J. L. Auriault and J. Lewandowska, Transp. Porous Media **16**, 31 (1994).
[37] R. G. Bentsen, Transp. Porous Media **14**(1), 23 (1994).
[38] R. G. Bentsen and A. A. Manai, Transp. Porous Media **11**(3),

243 (1993).
[39] P. A. Goode and T. S. Ramakrishnan, AIChE J. **39**(7), 1124 (1993).
[40] W. G. Gray, Adv. Water Resour. **6**, 130 (1983).
[41] W. G. Gray, Adv. Water Resour. **25**(8–12), 1091 (2002).
[42] W. G. Gray and S. M. Hassanizadeh, Int. J. Multiphase Flow **15**(1), 81 (1989).
[43] W. G. Gray and S. M. Hassanizadeh, Adv. Water Resour. **21**(4), 261 (1998).
[44] W. G. Gray and P. C. Y. Lee, Int. J. Multiphase Flow **3**, 333 (1977).
[45] H. K. Dahle and M. A. Celia, Comput. Geosci. **3**, 1 (1999).
[46] R. J. Held and M. A. Celia, Adv. Water Resour. **24**, 325 (2001).
[47] B. J. Bourbiaux and F. Kalaydjian, SPERE **5**, 361 (1990).
[48] J. S. Archer and S. W. Wong, Soc. Pet. Eng. J. **12**, 343 (1973).
[49] F. J. M. Kalaydjian, " in *67th Annual Technical Conference and Exhibition of the Society of Petroleum Engineers*, Richardson, TX, 1992, Society of Petroleum Engineers, pp. 491–506.
[50] Q. J. Liang and J. Lohrenz, Transp. Porous Media **15**, 71 (1994).
[51] C. Zarcone and R. Lenormand, C. R. Acad. Sci., Ser. IIb: Mec., Phys., Chim., Astron. **318**(11), 1429 (1994).
[52] D. G. Avraam, G. B. Kolonis, T. C. Roumeliotis, G. N. Constantinides, and A. C. Payatakes, Transp. Porous Media **16**, 75 (1994).
[53] M. S. Valavanides, G. N. Constantinides, and A. C. Payatakes, Transp. Porous Media **30**, 267 (1998).
[54] M. S. Valavanides and A. C. Payatakes, Adv. Water Resour. **24**(3–4), 385 (2001).
[55] K. P. Saripalli, H. Kim, P. S. C. Rao, and M. D. Annable, Environ. Sci. Technol. **31**(3), 932 (1997).
[56] C. E. Schaefer, D. A. DiCarlo, and M. J. Blunt, Water Resour. Res. **36**(4), 885 (2000).
[57] P. A. Goode, "Momentum transfer across fluid-fluid interfaces in porous media: A network model," Ph.D. thesis, Heriot-Watt University, UK, (1991).
[58] G. R. McNamara and G. Zanetti, Phys. Rev. Lett. **61**(20), 2332 (1988).
[59] F. J. Higuera and J. Jiménez, Europhys. Lett. **9**, 663 (1989).
[60] U. Frisch, D. d'Humières, B. Hasslacher, P. Lallemand, Y. Pomeau, and J.-P. Rivet, Complex Syst. **1**, 649 (1987).
[61] U. Frisch, B. Hasslacher, and Y. Pomeau, Phys. Rev. Lett. **56**, 1505 (1986).
[62] J. F. Olson and D. H. Rothman, J. Fluid Mech. **341**, 341 (1997).
[63] J. H. Kinney, T. M. Breunig, T. L. Starr, D. Haupt, M. C. Nichols, S. R. Stock, M. D. Butts, and R. A. Saroyan, Science **260**, 789 (1993).
[64] K. Langaas and P. Papatzacos, Transp. Porous Media **45**, 241 (2001).
[65] K. S. Delibasis, G. K. Matsopoulos, N. A. Mouravliansky, and K. S. Nikita, Comput. Med. Imaging Graph. **25**, 343 (2001).
[66] W. E. Lorenson and H. E. Cline, Comput. Graph. **21**(4), 163 (1987).
[67] C. Zhou, R. Shu, and M. S. Kankanhalli, Comput. Graph. **19**(6), 793 (1995).
[68] J. McClure, C. Pan, D. Adalsteinsson, W. G. Gray, and C. T. Miller, in *Proceedings of the XVth International Conference on Computational Methods in Water Resources,Chapel Hill, NC, 2004* Elsevier, New York, 2004), pp. 23–35.
[69] M. Junk, A. Klar, and L.-S. Luo, J. Comput. Phys. (to be published).
[70] D. d'Humières, I. Ginzburg, M. Krafczyk, P. Lallemand, and L.-S. Luo, Philos. Trans. R. Soc. London, Ser. A **360**, 437 (2002.
[71] P. Lallemand and L.-S. Luo, Phys. Rev. E **61**(6), 6546 (2000).
[72] P. Lallemand and L.-S. Luo, J. Comput. Phys. **184**, 406 (2003).
[73] X. Shan and H. Chen, Phys. Rev. E **47**, 1815 (1993).
[74] C. Pan, M. Hilpert, and C. T. Miller, Water Resour. Res. **40**, W01501 (2004).
[75] N. Martys and H. Chen, Phys. Rev. E **53**, 743 (1996).
[76] X. Shan and G. Doolen, Phys. Rev. E **54**(4), 3614 (1996).
[77] X. Shan and G. Doolen, J. Stat. Phys. **81**(1/2), 379 (1995).
[78] C. Pan, J. F. Prins, and C. T. Miller, Comput. Phys. Commun. **158**(2), 89 (2004).
[79] I. Ginzburg and D. d'Humières, Phys. Rev. E **68**, 066614:1–30 (2003).
[80] C. Pan, L.-S. Luo, and C. T. Miller, Comput. Fluids (to be published).
[81] J. Chin, E. S. Boek, and P. V. Coveney, Philos. Trans. R. Soc. London **360**, 647 (2002).
[82] R. R. Nourgaliev, T. N. Dinh, T. G. Theofanous, and D. Joseph, Int. J. Multiphase Flow **29**, 117 (2003).
[83] F. A. L. Dullien, *Porous Media: Fluid Transport and Pore Structure* (Academic, San Diego, 1992).
[84] R. G. Bentsen and A. A. Manai, Transp. Porous Media **11**, 243 (1993).